

# Electron enrichment of armchair graphene nano-ribbons increases stability and induces Fermi level pinning

E. Louis<sup>1,2,\*</sup>, E. San-Fabián<sup>2,3</sup>, G. Chiappe<sup>1,2</sup>, J.A. Vergés<sup>2,4</sup>

<sup>1</sup>*Departamento de Física Aplicada, Universidad de Alicante, 03690 Alicante, Spain*

<sup>2</sup>*Instituto Universitario de Materiales de Alicante (IUMA) and Unidad Asociada del Consejo Superior de Investigaciones Científicas, Universidad de Alicante, 03690 Alicante, Spain*

<sup>3</sup>*Departamento de Química Física, Universidad de Alicante, E-03080 Alicante, Spain.*

<sup>4</sup>*Departamento de Teoría y Simulación de Materiales, Instituto de Ciencia de Materiales de Madrid (CSIC), Cantoblanco, 28049 Madrid, Spain.*

---

## Abstract

Molecular orbitals strongly localised at zig-zag edges of neutral armchair-GNRs (AGNRs) may act as free radicals that can capture electrons during ribbon processing, increasing ribbon's stability. Thus, it is mandatory investigating the charging process and its consequences. Unrestricted Density Functional Theory (DFT) calculations of short ribbons' total energy show that ribbon's charging is feasible. Energies calculated by Pariser-Parr-Pople (PPP) Hamiltonian solved within the Unrestricted Hartree-Fock (UHF-PPP) are compatible with DFT. Results for neutral ribbons indicate that: i) the fundamental gap of spin polarised (non-polarised) solutions is substantially larger (smaller) than experimental data, ii) the ground state is spin polarised, not observed experimentally. Charging introduces significant changes: a) total energy decreases with the number of captured electrons reaching a minimum, b) the ground state is not spin polarised, c) the fundamental gap is in-between that of spin polarised and non-polarised solutions of neutral ribbons, and, d) while in neutral ribbons valence and conduction band onsets plotted vs. the fundamental gap, linearly and symmetrically approach the mid-gap with slope 0.5, charging breaks this symmetry inducing Fermi level pinning as the band gap decreases; the slopes of the valence and conduction bands being  $\approx 0.0$  and  $1.0$ , respectively, in agreement with experiments.

---

\*Corresponding author. E-mail: enrique.louis@ua.es (Enrique Louis)

Table 1: Calculated total energies (all in eV) of small AGNR-[m,n] referred to the energy of the respective neutral ribbon. Calculations were carried out by means of either DFT with the functional/basis set B3LYP/6-31+G\*-SD, UHF-PPP or PM6. Charge at which energy is minimal in each case is shown in bold characters. Note that DFT energies are always smaller than those obtained with the mean field solution of the model Hamiltonian.

Charge	DFT		PPP		PM6		
	m = 14	m = 20	m = 14	m = 20	m=14	m=20	
n=7	2	<b>-3.32</b>	<b>-3.76</b>	<b>-2.82</b>	<b>-3.22</b>	<b>-3.68</b>	-4.02
	4	1.92	-0.90	3.25	0.61	-0.38	-3.03
	6	14.63	8.52	17.90	10.91	10.61	4.71
	8	32.10	23.95	39.65	27.85	29.13	17.91
n=9	2	<b>-3.39</b>	<b>-3.79</b>	<b>-1.38</b>	<b>-3.02</b>	<b>-2.84</b>	3.13
	4	0.18	-2.33	1.95	-0.26	-1.47	<b>-3.30</b>
	6	11.62	5.58	14.42	8.65	8.02	3.51
	8	28.92	19.93	34.09	23.96	23.70	15.19
n=15	2	<b>-3.98</b>	<b>-4.88</b>	<b>-1.33</b>	-1.33	<b>-5.92</b>	-6.20
	4	-2.81	-4.74	-0.81	<b>-2.03</b>	-5.48	<b>-6.62</b>
	6	4.34	0.13	7.12	3.24	0.59	-3.31
	8	18.15	10.26	21.91	14.45	12.19	5.12

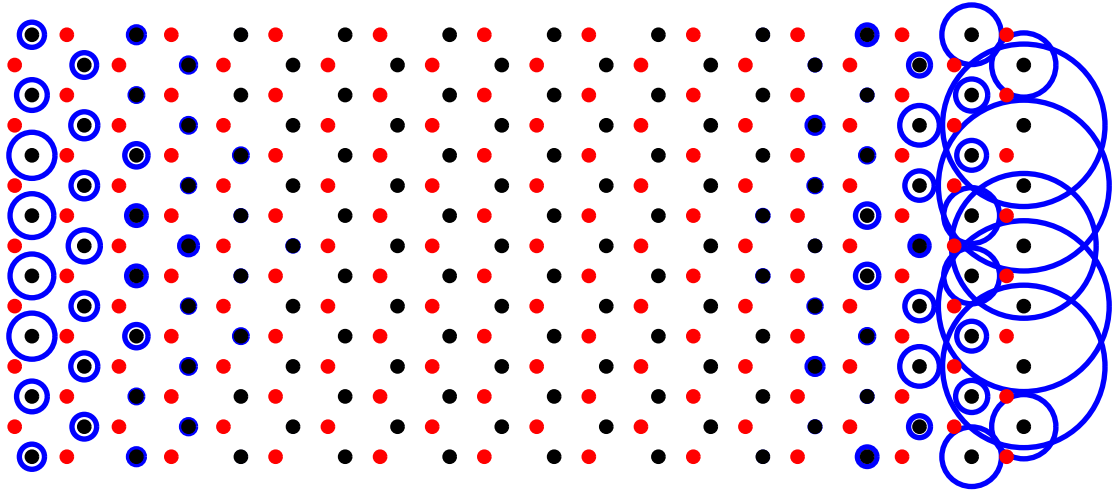
## 1. Introduction

The discovery of graphene has triggered a wealth of studies, both at research and production Institutions, aiming to find out applications for such a novel material [8, 21, 37]. Possible applications cover many industrial sectors requiring a panoply of properties that may justify referring to graphene as "the miracle material". Requirements go from being a defect free well-defined gap material as in most applications related to nano- and micro-electronics [28, 15] up to the unavoidable functionalisation of graphene if the aim is to use this material in any kind of chemical reaction (catalysis, sensors, electrochemistry,...) [8].

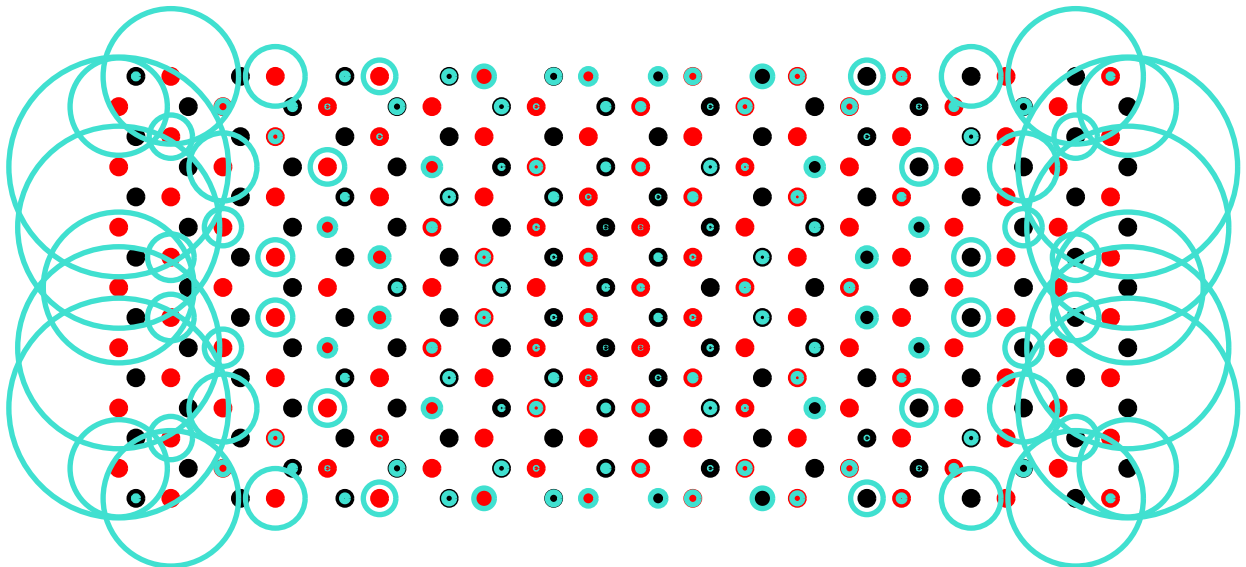
Controlled functionalisation usually requires starting from defect-free pieces of graphene. Thus, applications in the two industrial sectors mentioned above utilise preferably "perfect" ribbons. In the last few years bottom-up techniques have succeeded in producing nearly perfect Graphene Nano-Ribbons (GNR) very particularly Armchair Graphene Nano-Ribbons (AGNR). Bottom-up fabrication strategies, that rely on the coupling and subsequent cyclo-dehydrogenation of suitable precursor molecules on a metallic surface (mostly gold surface)[28, 15, 29, 31, 34, 30, 16, 25, 5, 24, 19, 13, 3] have been developed up to the point that ribbons with well-defined shape and dimensions, and thus, forbidden gap, can now be produced in many laboratories [15]. In addition, transferring the GNR by means of a STM tip to a thin NaCl deposit onto the metallic substrate has allowed a reliable characterisation of the electronic structure of the GNR. According to the authors [28] the whole process neither deform nor changes the charge-state of the ribbons.

Albeit finite GNRs show both arm-chair and zig-zag edges, a particular ribbon is named either AGNR or ZGNR according to the direction along which it is longer. The AGNR commonly used in experimental studies are usually much longer (along the arm-chair direction) than wider, therefore, no ambiguity is possible. Zig-zag edges of graphene nanostructures host localised electronic states [12, 20] that are predicted to be spin-polarised [32, 33, 10]. However, spin polarisation in these edges has never been observed. It is argued that such localised states may induce defect formation, edge roughness,..., interacting with the substrate and, as a consequence, complicating the study (both experimental and theoretical) of their intrinsic electronic and magnetic structure. As remarked in [35] "the armchair edges and the region surrounding them are substantially *more aromatic*, compared to zigzag edges". This is probably the origin of the much less technological difficulties that the fabrication of AGNR seems to pose, as compared to ZGNR. Molecular orbitals localised at zig-zag edges of neutral AGNR may act as free radicals that can capture electrons during ribbon processing, increasing ribbon's stability.

It is obvious that, although no experimental evidence of charge capture by AGNR is yet available (see Ref.[28]) the foregoing remarks make mandatory the investigation of the charging process and its consequences. In this work, electron charging of freely suspended "perfect" AGNR is investigated. Calculating the total energy of a ribbon with a



NEUTRAL NANORIBBON  
 SPIN UP PROBABILITY DENSITY  
 SPIN DOWN: RIGHT-LEFT SWAP



EXCESS CHARGE,  $Q=4$

Figure 1: (Color online) Upper panel: Spin probability density of a neutral 15-AGNR-(20,15) with total  $S_z = 0$ . Lower panel: local charge distribution of the same ribbon with an excess charge  $Q=4$ . In the neutral ribbon, antiferromagnetic order ( $S_z$  opposite at the two zig-zag edges) shows up breaking spatial inversion symmetry. Calculations were carried out by solving the PPP Hamiltonian within the UHF approximation.

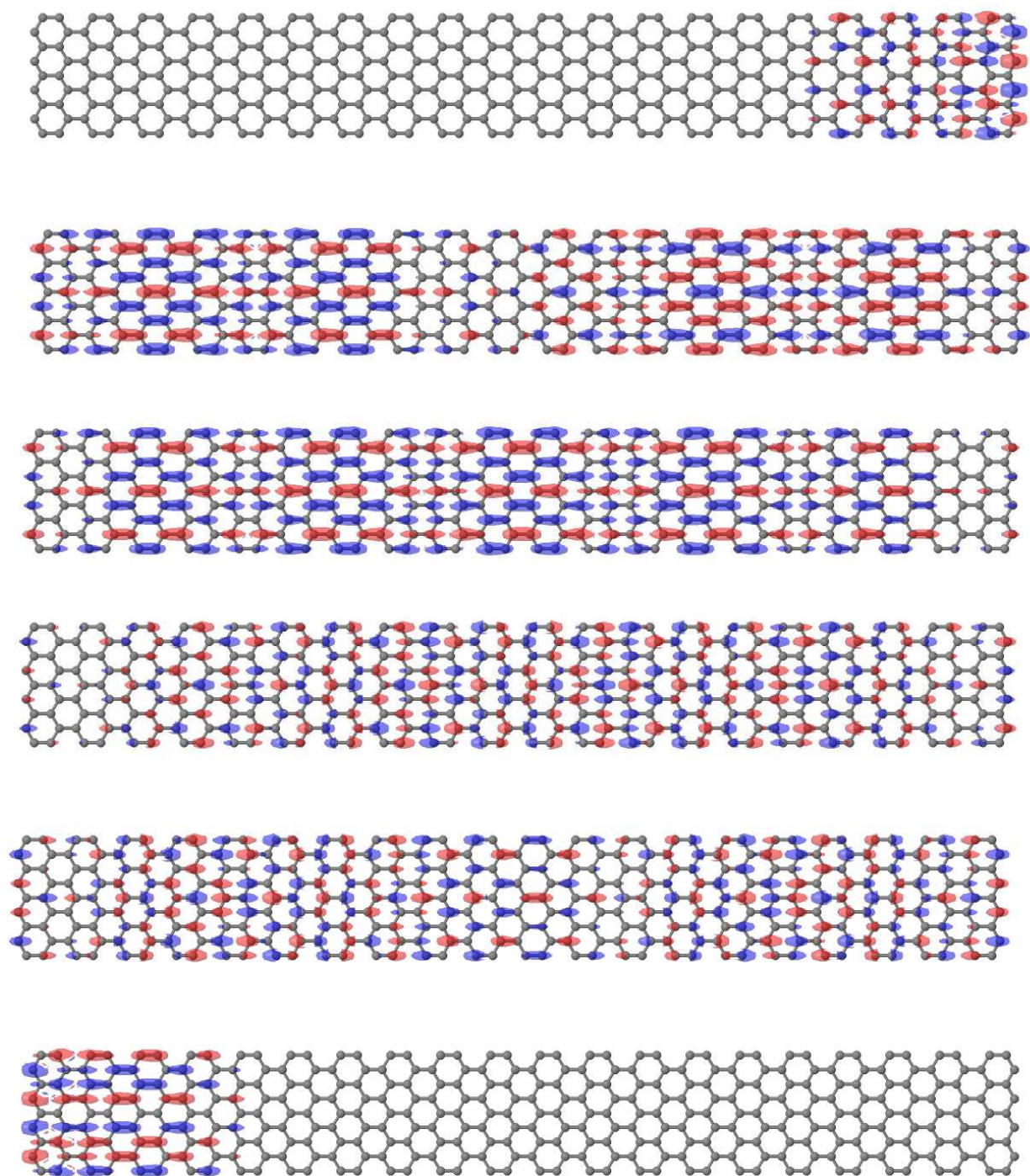


Figure 2: (Color online) Six spin up molecular orbitals around the Fermi level of a neutral 9-AGNR-[40,9]. Uppermost and lowermost orbitals are strongly localised at the zig-zag edges of the ribbon. The fundamental gap lies between the 3rd and fourth orbitals (starting from the lowermost orbital). The Fermi level lies midway between those two orbitals, its energy being -3.456 eV. Orbital energies, as calculated by means of UHF-PPP, are: -5.68, -5.62, -5.477, -1.453, -1.31 and -1.25 eV. Spin down orbitals are obtained from the spin up orbitals by right-left swapping.

given size (i.e.  $\{m, n\}$ ,  $m$  and  $n$  being the armchair and the zig-zag directions, respectively) versus the amount of charge it may capture, we obtain in all cases a curve with a single minimum that gives the most probable charged state of the nano-ribbon. Total energies were first calculated for small ribbons by means of *spin polarised* Density Functional Theory (DFT) and the Pariser-Parr-Pople PPP model Hamiltonian solved within the Unrestricted Hartree-Fock (UHF) approximation. As total energies calculated by means of the PPP model are compatible with DFT results, PPP was used in most cases thereafter.

The following charging induced results presented in this work do agree with observed features of AGNR: i) Absence of spin polarisation at zig-zag edges, and, ii) while in neutral ribbons valence and conduction band onsets (HOMO and LUMO levels) plotted vs. the fundamental gap, linearly and symmetrically approach the mid-gap with slope 0.5, charging breaks this symmetry inducing Fermi level pinning [17] as the band gap decreases; the slopes of the valence and conduction bands being close to  $\approx 0.1$  and  $0.9$ , to be compared with the experimental data,  $0.08$  and  $0.92$ , respectively.

## 2. Methods and numerical procedures

Calculations have been carried out on freely suspended AGNR- $\{m, n\}$ , also denominated in brief as  $n$ -AGNR, having a total number of carbons  $N_C = m \times n$ . The chosen ribbons widths were  $n=7, 9, 13, 15$  and  $19$ , while the largest length was  $m=100$  that corresponds to  $204.5 \text{ \AA}$  (only for the narrower ribbons). Largest ribbons were formed by around 1500 carbon atoms. Extra electrons were always added in pairs to preclude spin polarised ground states. Actually, we carried out calculations for  $Q=2, 4, 6$  and  $8$ . Dangling bonds of all carbon atoms at the ribbon edges have been bonded to hydrogen so that all carbons have a single non-saturated  $\pi$ -like orbital. Calculations were carried out by means of two semi-empirical methods, namely, PM6 and PPP. For the smallest systems calculations at the unrestricted DFT level have also been carried out. As regards the exchange-correlation functional, the widely accepted B3LYP[1, 14, 2, 22] functional in combination with the 6-31+G\*[11, 6] basis set has been used, which incorporates diffuse functions for the atoms, necessary to describe the delocalized behavior of the anions. Geometries of all ribbons have been optimised. The calculations were done with the Gaussian09 package [9].

PM6 [23] is the latest parametrisation of the NDDO method [7], which has been modified adopting Voityuk's core-core diatomic interaction parameters together with the method of parameter optimization. Parametrization including 70 elements and the heats of formation for a subset of 1,373 compounds (with only H, C, N, O, F, P, S, Cl and Br elements) give an average unsigned error (4.4 kcal/mol $-1$ ) better than alternative semiempirical methods, such as RM1(5.0), AM1(10.0) and PM3(6.3), or the HF/6-31G\*(7.4) and B3LYP/6-31G\*(5.2). The geometry of all systems was also optimised. The PPP Hamiltonian was solved within unrestricted Hartree-Fock approximation (UHF) using parameters fitted to the electronic structure of small PAH (see [27] and Supplementary data). Note that the fact that this Hamiltonian includes a single orbital per site should not be a major drawback as in graphene all carbons have a single non-saturated  $\pi$ -like orbital.

## 3. Results and Discussion

Probably forced by the extensive experimental evidence, most theoretical studies of AGNR have discarded unrestricted spin polarised solutions from the very beginning [36, 26]. This is so despite of the fact that mono-determinantal unrestricted solutions are spin polarised no matter the chosen framework, model Hamiltonians solved within Unrestricted Hartree-Fock, or the most sophisticated *ab initio* DFT and GW approaches [28, 32, 33, 10]. In the following we discuss an alternative way to reconcile the experimental evidence with calculations.

### 3.1. Localised states at the zig-zag edges

As pointed out in the Introduction, the zig-zag edges of neutral AGNR host unpaired electrons described by localised states that act as radical centers ready to capture charge. This is clearly illustrated in Fig. 1 which shows that the staggered magnetization in a neutral 15-AGNR- $\{20, 15\}$  is mostly localised at the two zig-zag edges of the ribbon. In the Figure only the up component of the spin is shown, the down component is derived from it by exchanging sides which illustrates the breaking of the specular symmetry with respect to the plane perpendicular to the C-C bonds that splits the ribbon in two identical parts. If electrons are incorporated to the ribbon, no matter how they were captured,

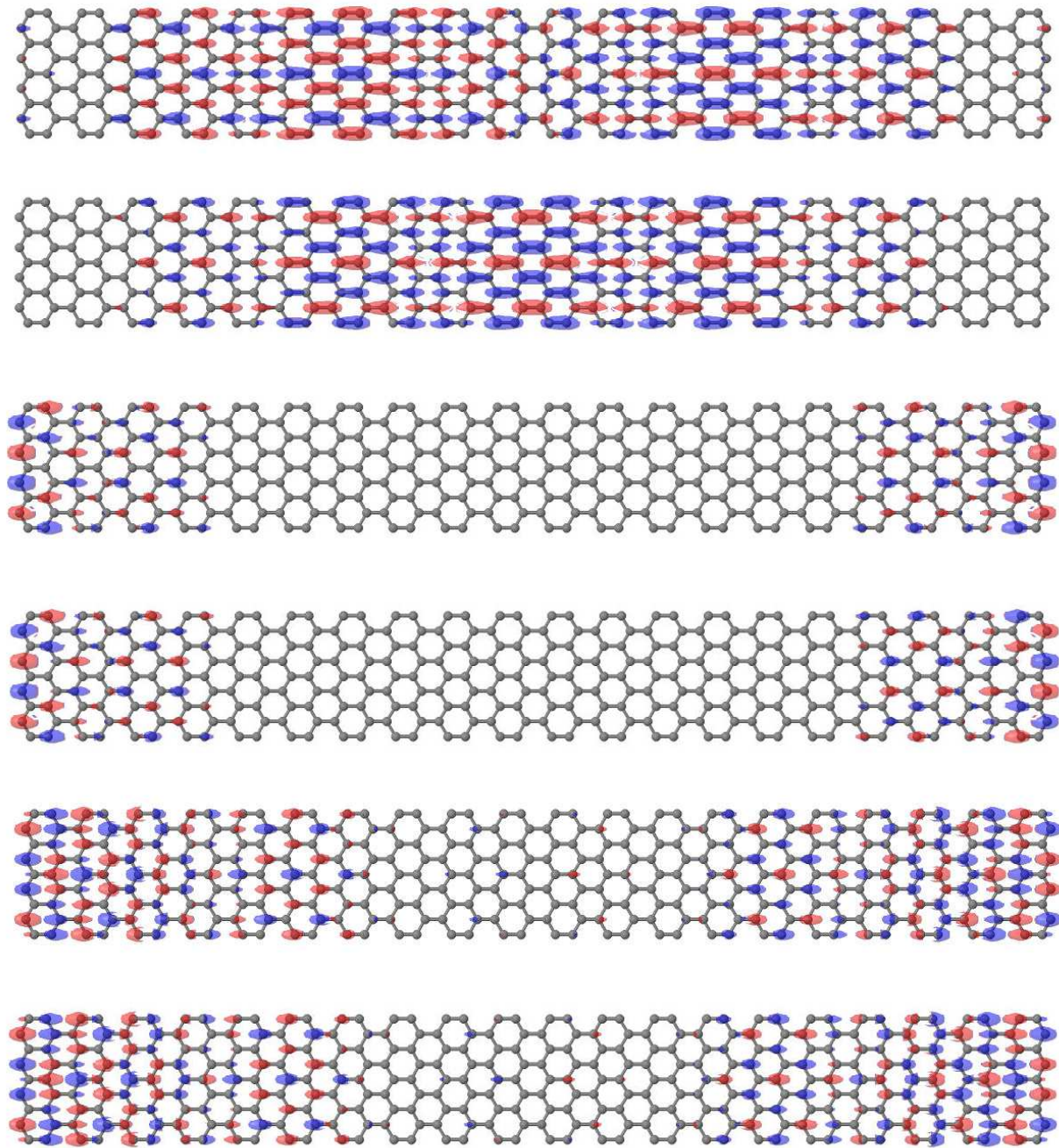


Figure 3: (Color online) Six spin up molecular orbitals around the Fermi level of a 9-AGNR-[40,9] charged with  $Q=2$ . The fundamental gap lies between the 4th the 5th orbitals (starting from the lowermost orbital). The Fermi level lies midway between those two orbitals, its energy being  $-1.27$  eV. Orbital energies, as calculated by means of UHF-PPP, are:  $-3.73$ ,  $-3.73$ ,  $-2.14$ ,  $-2.14$ ,  $-0.41$  and  $-0.067$  eV. Both  $S_z$  and  $S^2$  are null (non-magnetic configuration).

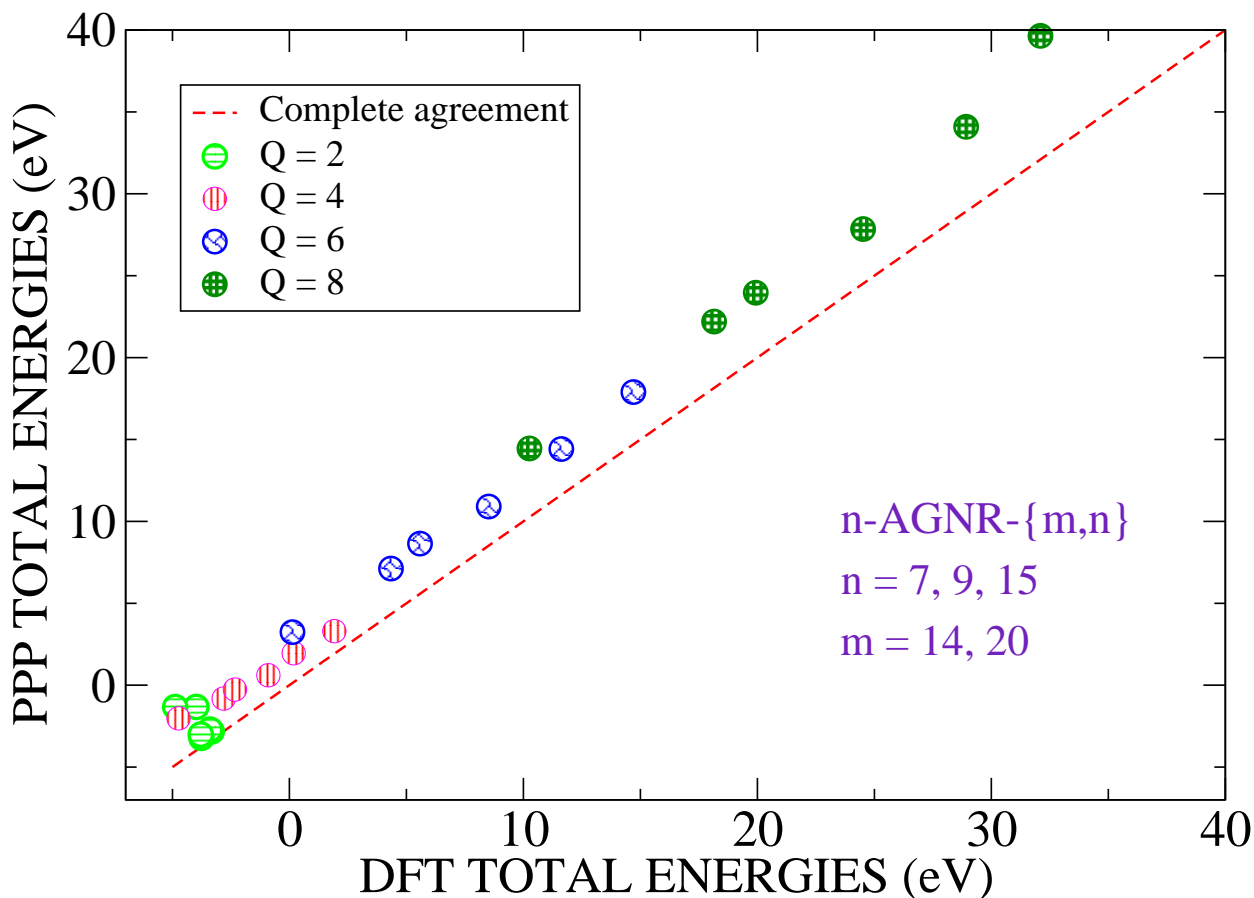


Figure 4: (Color online) Energies of charged  $n$ -AGNR- $\{m,n\}$  referred to that of the respective neutral ribbons, calculated by means of HF-PPP versus those obtained within the DFT framework and the combination functional/wavefunction set B3LYP/6-31+G\*-SD. The results correspond to ribbons charged with  $Q = 2, 4, 6, 8$  and sizes  $m = 14$  and  $20$  and  $n = 7, 9$  and  $15$ . (see Table 1).

the ribbon ground state becomes non-magnetic restoring the original symmetry of the ribbon (see lower panel of Fig. 1). In order to identify the energies at which these localised states lie, we have calculated what we call Partial Local Density of States (PLDOS) and plotted against the energy. PLDOS is calculated by summing up the local density on the carbon atoms within the unit cells at the left and right zig-zag edges of a  $n$ -AGNR. The results for the PLDOS in 19-AGNR neutral and charged with  $Q = 2$  and  $6$  electrons indicate that: In the neutral ribbon the Fermi level lies close to eigenstate at  $-3.5$  eV and just around  $-1.0$  eV two empty peaks are seen which correspond to empty orbitals localised at the zig-zag edges. Adding charge gradually fills these states in such a way that, for  $6$  excess electrons, localised empty states are far from the Fermi level.

This appealing characteristic of neutral spin polarised AGNR is better illustrated by the spin densities of the six molecular orbitals around the Fermi level (see Fig. 2) in a neutral 9-AGNR- $\{40,9\}$ . First and sixth orbitals (starting from the lowermost level) are strongly localised at the zig-zag edges of the ribbon. The Fermi level lies between the 3rd and fourth orbitals, its energy being  $-3.456$  eV. Molecular orbital energies calculated by means of UHF-PPP are:  $-5.68, -5.62, -5.477, -1.453, -1.31$  and  $-1.25$  eV. As already remarked, spin down orbitals are obtained from the spin up orbitals by exchanging sides. This illustrates the asymmetric character of these molecular orbitals. Actually, this asymmetry should affect the whole set of molecular orbitals, as illustrated in Fig. 2 (see 2nd up to 5th orbitals) and, as already pointed out, is due to the antiferromagnetic character of the ground state in neutral AGNR. The recovery of the full symmetry induced by charging the ribbons is nicely illustrated in Fig. 3. This Figure shows the spin densities of six spin up molecular orbitals around the Fermi level of a 9-AGNR- $\{40,9\}$  charged with  $Q=2$ . Both  $S_z$  and  $S^2$  are

null (non-magnetic configuration). The original symmetry of the graphene lattice has been fully restored. Third and Fourth orbitals are strongly localised at the zig-zag edges of the ribbon. The Fermi level lies between the 4th and fifth orbitals. Orbital energies, as calculated by means of UHF-PPP, are: -3.73, -3.73, -2.14, -2.14, -0.41 and -0.067 eV.

### 3.2. Charging stabilises AGNR

At this point the issue is whether charging reduces the nano-ribbon total energy and, thus, increases its stability. Calculated total energies (all in eV) of small AGNR- $\{m,n\}$  by means of DFT, UHF-PPP and PM6, are reported in Table 1. As shown in the Table, whenever the excess charge is not too high, charged ribbons are more stable than neutral ribbons. This result, which is the core of the present work, holds for the three theoretical methods used here. In addition it is noted that DFT energies are always smaller than those obtained with the UHF solution of the model PPP Hamiltonian. Instead, no conclusion can be derived from a comparison of DFT and MP6 results. Anyway, the main result is very robust as the three theoretical methods used here always agree at a qualitative and, in some cases, even at a semi-quantitative level: the total energy of AGNR diminishes upon ribbon's charging reaching a minimum at a charging level that depends on ribbon's length and width. Thereafter, the energy increases monotonically. Charge at which energy is minimal in each case is shown in bold characters in Table 1.

Aiming to illustrate in a pictorial way the agreement of DFT and HF-PPP results, Figure 4 depicts the energies of charged  $n$ -AGNR- $\{m,n\}$  referred to that of the respective neutral ribbons. The results correspond to ribbons charged with  $Q = 2, 4, 6, 8$  and sizes  $m = 14$  and  $20$  and  $n = 7, 9$  and  $15$ . (see Table 1). The straight line corresponds to complete agreement, that is, all DFT energies coinciding with all UHF-PPP energies. Note that the numerical data are not far from this *ideal* line validating the use of HF-PPP for the calculation of total energies, fundamental gaps, .. etc. Additional results obtained with PPP reinforce the main conclusion of the present work, namely, charging stabilises AGNRs.

Figure 5 reports the total energies (all in eV) for several AGNR as a function of the excess charge  $Q$ . In the upper panel results for 7-AGNR and five lengths  $m=20, 30, 40, 60, 80$  and  $100$  (actual lengths excluding hydrogens are, 40.89, 61.34, 122.67, 163.56 and 204.45 Å). The significant dependence on ribbon length of the charge that a given ribbon can admit is clearly illustrated by these results. The middle panel depicts some results obtained with the semi-empirical method PM6. They illustrate clearly the tendency of PM6 to give energy minima deeper than the other two methods. These results, together with those discussed above highlight that charge stabilisation of the ribbon for a given excess charge  $Q$  increases with both length and width.

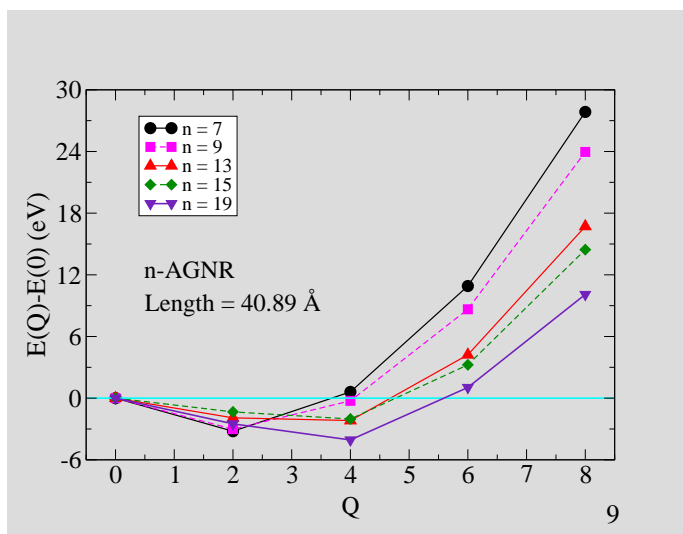
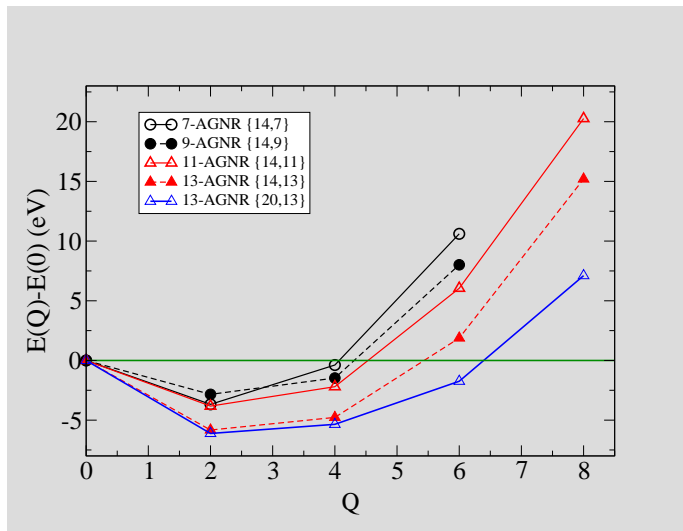
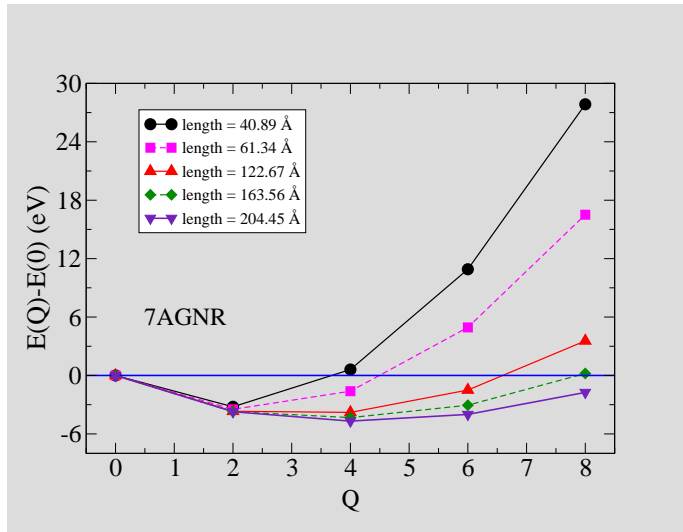


Figure 5: (Color online) Total energies (all in eV) of several charged AGNR as a function of charge  $Q$ . Upper: 7-AGNR and five lengths  $m=20$ , 40, 60, 80 and 100 (actual lengths excluding hydrogens are, 40.89, 81.78, 122.67, 153.56 and 204.45 Å). Middle: Results for  $n=7, 9, 11$  and  $13$  of two lengths versus the excess charge. Lower: Results for AGNRs of a fixed length  $m=20$  and five widths  $n=7, 9, 13, 15$  and  $19$ , obtained with PPP. Total energies, referred to that of the corresponding neutral ribbon, were calculated with PPP (upper and lower) or PM6 (middle). This Figure clearly illustrates the dependence of charging and its effects on ribbons width and length.

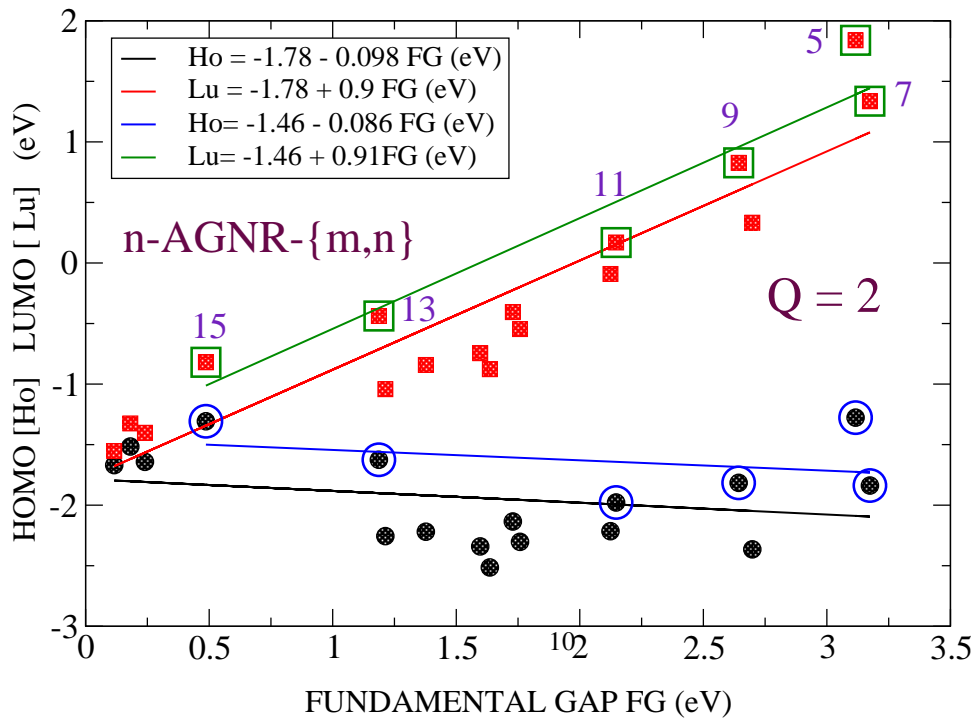
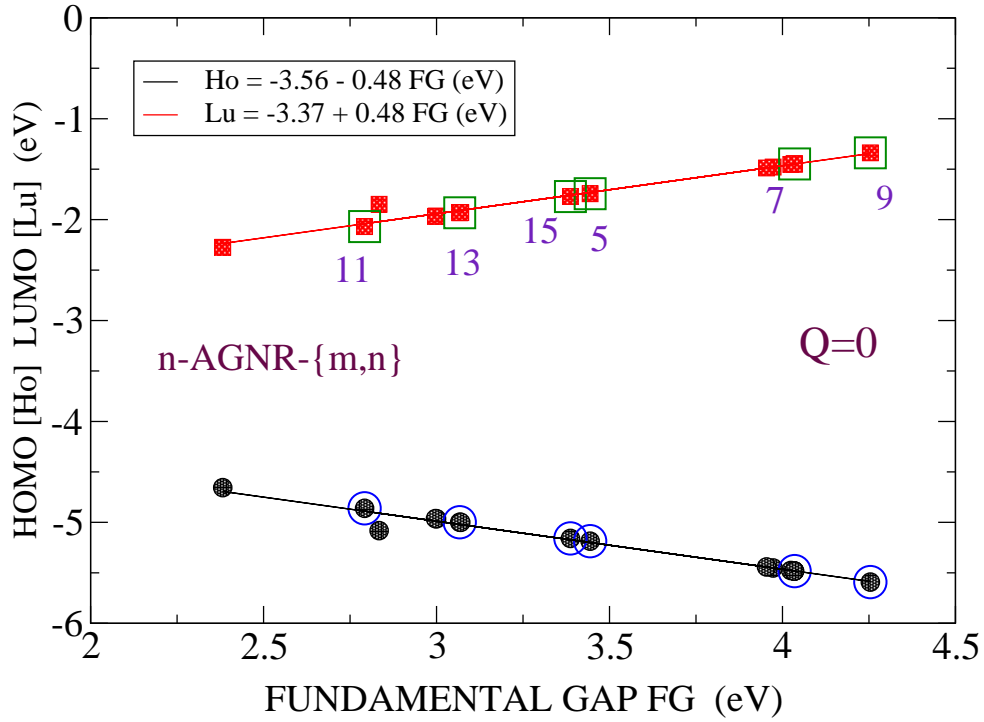


Figure 6: (Color online) HOMO (filled circles) and LUMO (filled squares) versus Fundamental gap for armchair ribbons of width  $n=5, 7$  and  $9$  and lengths of  $40.9, 81.8, 122.7$  and  $163.6 \text{ \AA}$ , and of width  $n=11, 13, 15$  and  $19$  and lengths of  $40.9$  and  $81.8 \text{ \AA}$ . Large symbols correspond to ribbons that measure  $40.9 \text{ \AA}$  in length. The straight lines fitted to the numerical results are shown in the inset. Calculations were carried out with UHF-PPP on neutral ribbons  $Q=0$  (upper) and with an excess charge of  $2$  electrons (lower).

### 3.3. Fundamental gap of neutral and charged AGNR versus ribbon width and length

The upper panel of Figure 6 depicts results for the HOMO (filled circles) and LUMO (filled squares) versus the fundamental gap (FG) for neutral AGNRs of several widths and lengths. Results, obtained with HF-PPP, correspond to widths of  $n=5, 7$  and  $9$  and lengths of  $40.9, 81.8, 122.7$  and  $163.6$  Å, and widths of  $n= 11, 13, 5$  and  $19$  and lengths of  $40.9$  and  $81.8$  Å. Empty symbols correspond to ribbons of fixed length ( $40.9$  Å). Both HOMO and LUMO show a monotonic dependence on ribbon's FG and a very irregular dependence on ribbon's width. The straight lines fitted to the numerical results are shown in the inset. The slopes are very close to  $S=\pm 0.5$  (valence and conduction band, respectively), as expected in a system with electron-hole symmetry [17].

Recent experiments [17] on AGNRs of several widths deposit on Au(1,1,1) surface report results at variance with the symmetric case illustrated in the upper panel of Figure 6. The authors presented results for the valence and conduction bands versus the fundamental gap that for FG larger than  $1.7$  eV, vary linearly with ribbon's FG with slopes of approximately  $\pm 0.5$ , as found in a symmetric system. However, for  $FG < 1.7$  eV, the valence band show Fermi level pinning as the fundamental band gap decreases. The slope of the fitted straight line being slightly smaller than  $0.1$ . In addition, the conduction band is inversely proportional to the ribbon's width (see Fig. 7). Similar results are obtained here for freely suspended ribbons charged with two extra electrons. Again, calculations were carried out with HF-PPP. The results depicted in the lower panel of Figure 6 correspond to ribbons of width and length equal to those used for neutral ribbons. The straight lines fitted to the numerical results are shown in the inset. When all numerical results are included in the fittings, the slopes are  $-0.098$  and  $0.9$  for HOMO and LUMO, respectively, not far from the results reported in Ref. [17] namely,  $-0.08 \pm 0.05$  and  $0.92 \pm 0.05$ . Results do not change much if fittings are carried out including only data for ribbons of length  $40.9$  Å. These slopes were obtained from fittings of data with  $FG < 3.2$  eV, higher than the experimental value of  $1.7$  eV, a discrepancy likely due to the mean field approach adopted here. On the other hand, the results shown in the lower panel of Fig. 6 reveal a monotonic dependence of the two bands on the ribbon's width, as opposed to what we obtained for neutral ribbons. This is further illustrated by Fig. 7 which shows that charged AGNR show a smooth dependence on both, length and width.

It is worth noting that a wide gap in neutral AGNR is only obtained if a spin-unrestricted formalism allowing spin symmetry breaking is used, something not yet fully supported by experiments. Instead, gaps in non-polarised ribbons are very small no matter which method is used in the calculations. The present results indicate that charging has several appealing effects: i) the ground state of the charged ribbons is non-polarised, ii) the gaps are substantially smaller than those found in spin-polarised solutions, although are larger than the experimental ones, and iii) Valence and Conduction bands are no longer symmetrically placed with respect to the Fermi level. We believe that these results are enough to justify the following of the route initiated in this work as at present there is no alternative theory that can explain the experimental results of Ref. [17].

## 4. Concluding Remarks

Zigzag edges of graphene nanoribbons, in particular AGNRs, host localised electronic states of opposite spin at both ribbon edges. Consequently, the most sophisticated quantum chemistry tools now available, predict a spin polarized ground state. However, spin polarised edge states have not yet been observed experimentally. This dramatic disagreement is usually ascribed to the high susceptibility of these states to develop edge defects and roughness, and interaction with the supporting substrate. In this work, taking for granted the predicted spin polarised character of zigzag edges in AGNRs and the reliability of the experimental studies that aiming to find any traces of spin polarisation have failed, we undertook the task of seeking alternative effects that may obscure or eliminate that spin polarisation. Taking note of the fact that some of the so called *edge states* may be empty, we consider the possibility that adding extra charge to the ribbons might contribute to increase their stability. Our work, then, was focused on this issue. All calculations, no matter which method we used, gave a curve of total energy versus extra charge that showed a minimum at a value of the charge that varied with ribbon's width and length. Width dependence of the fundamental gap reveals valence bands which show Fermi level pinning as the fundamental band gap decreases, in agreement with recent experimental data and at variance with the symmetry characteristic of neutral ribbons. It is pertinent to remark that it would be interesting to investigate the conductance of charged ribbons along the lines, for instance, of a recently published work [26]. As regards the actual values of the forbidden gap it is noted that, in neutral ribbons the gap of spin polarised gaps is larger than what has been observed up to now, the opposite occurs in non-polarised. Instead, charged ribbons show a forbidden gap in-between those two, closer to the experimental data.

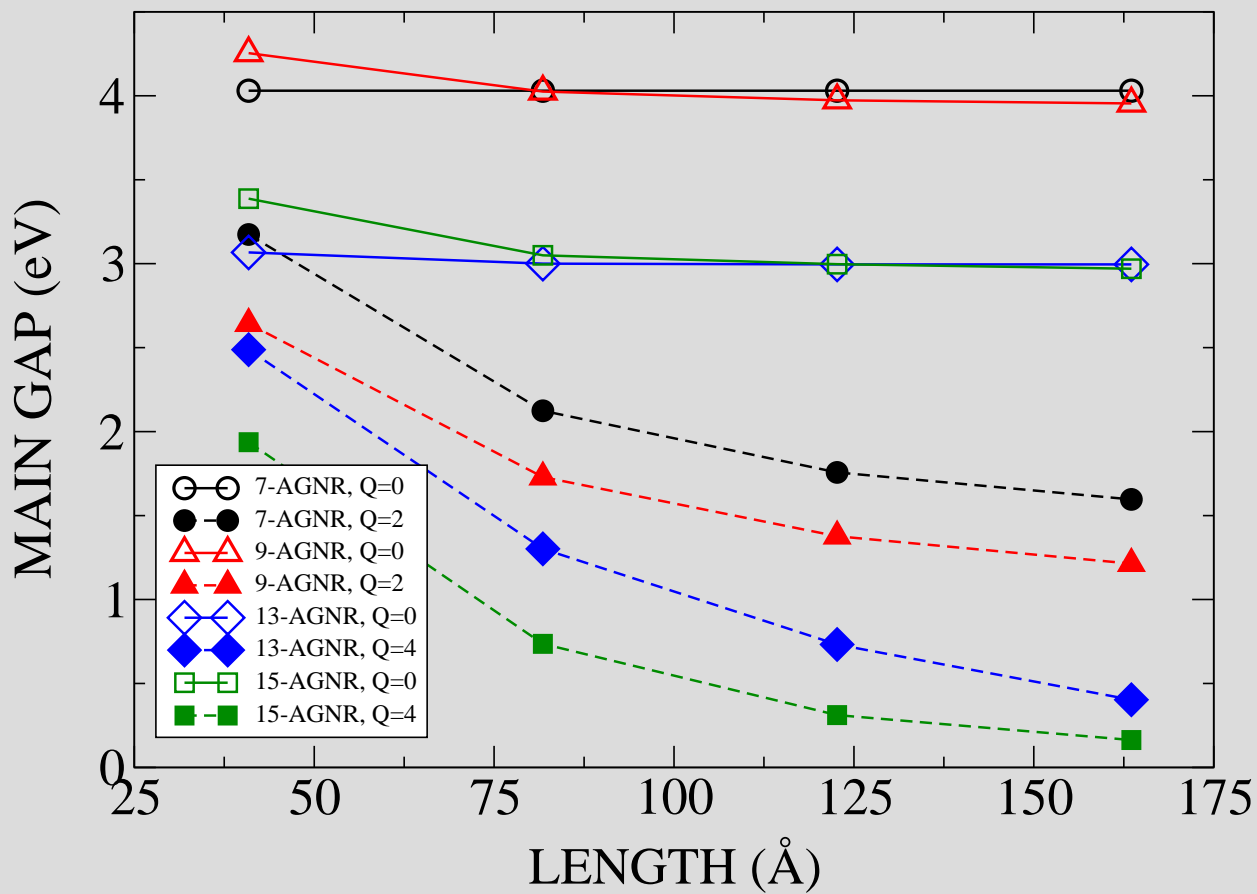


Figure 7: (Color online) Fundamental gap for neutral and charged AGNRs versus ribbon's length and several widths  $n = 7, 9, 13$  and  $15$ . Calculations were carried out with UHF-PPP. Neutral AGNRs shows a LUMO that varies irregularly with the ribbon's width, but depends linearly on length. Meanwhile, in charged ribbons both HOMO and LUMO vary linearly with length, as in neutral ribbons, albeit in this case the slopes are very different, being close to zero in the HOMO. The latter is associated to a pinning of the Fermi level.

Before ending it is worth to comment on recent theoretical and experimental work [4, 18] that presented sound evidence in the sense that Interfaces between topologically distinct GNRs, in particular they investigated 7/9-AGNR, are predicted to support half-filled, in-gap localized electronic states. We hope that the work presented here will be of some help in understanding and developing applications of such an interesting proposal.

### **Acknowledgments**

This work has been partially supported by the Spanish "Ministerio de Ciencia, Innovación y Universidades" (Grants FIS2015-64222-C2-1-P, FIS2015-64222-C2-2-P, MAT2016-77742-C2-2-P and AYA2015-66899-C2-2-P), and the Universidad de Alicante is gratefully acknowledged.

## BIBLIOGRAPHY

### References

- [1] A. D. Becke. Density-functional exchange-energy approximation with correct asymptotic behavior. *Phys. Rev. A*, 38(6):3098–3100, 1988.
- [2] Axel D. Becke. Density functional thermochemistry. iii. the role of exact exchange. *J. Chem. Phys.*, 98(7):5648–5652, 1993.
- [3] Patrick B. Bennett, Zahra Pedramrazi, Ali Madani, Yen-Chia Chen, Dimas G. de Oteyza, Chen Chen, Felix R. Fischer, Michael F. Crommie, and Jeffrey Bokor. Bottom-up graphene nanoribbon field-effect transistors. *Applied Physics Letters*, 103(25):253114, 2013.
- [4] Ting Cao, Fangzhou Zhao, and Steven G. Louie. Topological phases in graphene nanoribbons: Junction states, spin centers, and quantum spin chains. *Phys. Rev. Lett.*, 119:076401, Aug 2017.
- [5] Yen-Chia Chen, Dimas G. de Oteyza, Zahra Pedramrazi, Chen Chen, Felix R. Fischer, and Michael F. Crommie. Tuning the band gap of graphene nanoribbons synthesized from molecular precursors. *ACS Nano*, 7(7):6123–6128, 2013. PMID: 23746141.
- [6] T. Clark, J. Chandrasekhar, G. W. Spitznagel, and P. V. R. Schleyer. Efficient diffuse function-augmented basis sets for anion calculations. iii. the 3-21+g basis set for first-row elements, li- f. *J. Comput. Chem.*, 4(3):294 – 301, 1983.
- [7] M. J. S. Dewar and W. Thiel. Ground states of molecules. 38. the mndo method. approximations and parameters. *J. Am. Chem. Soc.*, 99:4899, 1977.
- [8] Ali Eftekhari and Hermenegildo Garcia. The necessity of structural irregularities for the chemical applications of graphene. *Materials Today Chemistry*, 4:1 – 16, 2017.
- [9] M. J. Frisch, G. W. Trucks, H. B. Schlegel, G. E. Scuseria, M. A. Robb, J. R. Cheeseman, G. Scalmani, V. Barone, B. Mennucci, G. A. Petersson, H. Nakatsuji, M. Caricato, X. Li, H. P. Hratchian, A. F. Izmaylov, J. Bloino, G. Zheng, J. L. Sonnenberg, M. Hada, M. Ehara, K. Toyota, R. Fukuda, J. Hasegawa, M. Ishida, T. Nakajima, Y. Honda, O. Kitao, H. Nakai, T. Vreven, J. A. Montgomery, Jr., J. E. Peralta, F. Ogliaro, M. Bearpark, J. J. Heyd, E. Brothers, K. N. Kudin, V. N. Staroverov, R. Kobayashi, J. Normand, K. Raghavachari, A. Rendell, J. C. Burant, S. S. Iyengar, J. Tomasi, M. Cossi, N. Rega, J. M. Millam, M. Klene, J. E. Knox, J. B. Cross, V. Bakken, C. Adamo, J. Jaramillo, R. Gomperts, R. E. Stratmann, O. Yazyev, A. J. Austin, R. Cammi, C. Pomelli, J. W. Ochterski, R. L. Martin, K. Morokuma, V. G. Zakrzewski, G. A. Voth, P. Salvador, J. J. Dannenberg, S. Dapprich, A. D. Daniels, Ö. Farkas, J. B. Foresman, J. V. Ortiz, J. Cioslowski, and D. J. Fox. Gaussian 09 revision d.01, 2009. Gaussian Inc. Wallingford CT.
- [10] Michael Golor, Cornelia Koop, Thomas C. Lang, Stefan Wessel, and Manuel J. Schmidt. Magnetic correlations in short and narrow graphene armchair nanoribbons. *Phys. Rev. Lett.*, 111:085504, Aug 2013.
- [11] P. C. Hariharan and J. A. Pople. The influence of polarization functions on molecular orbital hydrogenation energies. *Theor. Chim. Acta*, 28:213, 1973.
- [12] Siegfried Hauptmann. The aromatic sextet: Von e. clar; john wiley & sons ltd, london, new york, sydney, toronto 1972; 128 seiten mit zahlreichen formelbildern; format 13 20 cm; broschiert £ 1, 50. *Zeitschrift fr Chemie*, 13(5):200–200, 1973.
- [13] Matthias Koch, Francisco Ample, Christian Joachim, and Leonhard Grill. Voltage-dependent conductance of a single graphene nanoribbon. *Nature Nanotechnology*, 7:713, oct 2012.
- [14] Chengteh Lee, Weitao Yang, and Robert G. Parr. Development of the colle-salvetti correlation-energy formula into a functional of the electron density. *Phys. Rev. B*, 37:785–789, Jan 1988.
- [15] Talirz Leopold, Ruffieux Pascal, and Fasel Roman. On-surface synthesis of atomically precise graphene nanoribbons. *Advanced Materials*, 28(29):6222–6231, 2016.
- [16] Suchun Li, Chee Kwan Gan, Young-Woo Son, Yuan Ping Feng, and Su Ying Quek. Anomalous length-independent frontier resonant transmission peaks in armchair graphene nanoribbon molecular wires. *Carbon*, 76:285 – 291, 2014.
- [17] Néstor Merino-Díez, Aran Garcia-Lekue, Eduard Carbonell-Sanromà, Jingcheng Li, Martina Corso, Luciano Colazzo, Francesco Sedona, Daniel Sánchez-Portal, Jose I. Pascual, and Dimas G. de Oteyza. Width-dependent band gap in armchair graphene nanoribbons reveals fermi level pinning on au(111). *ACS Nano*, 11(11):11661–11668, 2017. PMID: 29049879.
- [18] Daniel J Rizzo, Gregory Veber, Ting Cao, Christopher Bronner, Ting Chen, Fangzhou Zhao, Henry Rodriguez, Steven G Louie, Michael F Crommie, and Felix R Fischer. Topological band engineering of graphene nanoribbons. *Nature*, 560(7717):204–208, 2018.
- [19] Pascal Ruffieux, Jinming Cai, Nicholas C. Plumb, Luc Patthey, Deborah Prezzi, Andrea Ferretti, Elisa Molinari, Xinliang Feng, Klaus Mllen, Carlo A. Pignedoli, and Roman Fasel. Electronic structure of atomically precise graphene nanoribbons. *ACS Nano*, 6(8):6930–6935, 2012. PMID: 22853456.
- [20] Miquel Solà. Forty years of Clar’s aromatic  $\pi$ -sextet rule. *Frontiers in chemistry*, 1:22, oct 2013.
- [21] Pablo Solis-Fernandez, Mark Bissett, and Hiroki Ago. Synthesis, structure and applications of graphene-based 2d heterostructures. *Chem. Soc. Rev.*, 46:4572–4613, 2017.
- [22] P. J. Stephens, F. J. Devlin, C. F. Chabalowski, and M. J. Frisch. Ab initio calculation of vibrational absorption and circular dichroism spectra using density functional force fields. *J. Phys. Chem.*, 98(45):11623–11627, 1994.
- [23] James J. P. Stewart. Optimization of parameters for semiempirical methods v: Modification of nndo approximations and application to 70 elements. *Journal of Molecular Modeling*, 13(12):1173–1213, 2007.
- [24] Leopold Talirz, Hajo Sde, Jinming Cai, Pascal Ruffieux, Stephan Blankenburg, Rached Jafaar, Reinhard Berger, Xinliang Feng, Klaus Mllen, Daniele Passerone, Roman Fasel, and Carlo A. Pignedoli. Termini of bottom-up fabricated graphene nanoribbons. *Journal of the American Chemical Society*, 135(6):2060–2063, 2013. PMID: 23350872.
- [25] Leopold Talirz, Hajo Sde, Tim Dumsflaff, Shiyong Wang, Juan Ramon Sanchez-Valencia, Jia Liu, Prashant Shinde, Carlo A. Pignedoli, Liangbo Liang, Vincent Meunier, Nicholas C. Plumb, Ming Shi, Xinliang Feng, Akimitsu Narita, Klaus Mllen, Roman Fasel, and Pascal Ruffieux. On-surface synthesis and characterization of 9-atom wide armchair graphene nanoribbons. *ACS Nano*, 11(2):1380–1388, 2017. PMID: 28129507.
- [26] J. A. Vergés, G. Chiappe, Emilio San-Fabián, and E. Louis. Conductance through the armchair graphene nanoribbons 9-agnr: Strong dependence on contact to leads. *Phys. Rev. B*, 98:155415, Oct 2018.

- [27] J. A. Verges, E. SanFabián, G. Chiappe, and E. Louis. Fit of pariser-parr-pople and hubbard model hamiltonians to charge and spin states of polycyclic aromatic hydrocarbons. *Physical Review B*, 81(8):085120, FEB 2010 2010. PT: J; TC: 6; UT: WOS:000275053300047.
- [28] Shiyong Wang, Leopold Talirz, Carlo A Pignedoli, Xinliang Feng, Klaus Müllen, Roman Fasel, and Pascal Ruffieux. Giant edge state splitting at atomically precise graphene zigzag edges. *Nature Communications*, 7:11507, may 2016.
- [29] Wen-Xiao Wang, Mei Zhou, Xinqi Li, Si-Yu Li, Xiaosong Wu, Wenhui Duan, and Lin He. Energy gaps of atomically precise armchair graphene sidewall nanoribbons. *Phys. Rev. B*, 93:241403, Jun 2016.
- [30] Chun-Shian Wu and Jeng-Da Chai. Electronic properties of zigzag graphene nanoribbons studied by tao-dft. *Journal of Chemical Theory and Computation*, 11(5):2003–2011, 2015.
- [31] Wentao Xu and Tae-Woo Lee. Recent progress in fabrication techniques of graphene nanoribbons. *Mater. Horiz.*, 3:186–207, 2016.
- [32] Li Yang, Cheol-Hwan Park, Young-Woo Son, Marvin L. Cohen, and Steven G. Louie. Quasiparticle energies and band gaps in graphene nanoribbons. *Phys. Rev. Lett.*, 99:186801, Nov 2007.
- [33] Oleg V Yazyev. Emergence of magnetism in graphene materials and nanostructures. *Reports on Progress in Physics*, 73(5):056501, apr 2010.
- [34] Chia-Nan Yeh, Pei-Yin Lee, and Jeng-Da Chai. Electronic and Optical Properties of the Narrowest Armchair Graphene Nanoribbons Studied by Density Functional Methods. *Australian Journal of Chemistry*, 69(9):960–968, 2016.
- [35] Aristides D. Zdetsis and E. N. Economou. A pedestrian approach to the aromaticity of graphene and nanographene: Significance of huckels  $(4n+2)$  electron rule. *The Journal of Physical Chemistry C*, 119(29):16991–17003, 2015.
- [36] Aristides D. Zdetsis and E.N. Economou. Rationalizing and reconciling energy gaps and quantum confinement in narrow atomically precise armchair graphene nanoribbons. *Carbon*, 116:422 – 434, 2017.
- [37] Yanwu Zhu, Hengxing Ji, Hui-Ming Cheng, and Rodney S Ruoff. Mass production and industrial applications of graphene materials. *National Science Review*, 5(1):90–101, 2018.